Gene Signatures Associated with Mouse Postnatal Hindbrain Neural Stem Cells and Medulloblastoma Cancer Stem Cells Identify Novel Molecular Mediators and Predict Human Medulloblastoma Molecular Classification.

Submitted to Cancer Discovery

Gene signatures associated with mouse postnatal hindbrain neural stem cells and medulloblastoma cancer stem cells identify novel molecular mediators and predict human MB molecular classification.

Daniela Corno[1], Mauro Pala[2§], Manuela Cominelli[3§], Barbara Cipelletti[1], Ketty Leto[4], Laura Croci[5], Valeria Barili[5], Federico Brandalise[6], Raffaella Melzi[7], Alessandra Di Gregorio[4], Lucia Sergi Sergi[8], Letterio Salvatore Politi[9], Lorenzo Piemonti[7], Alessandro Bulfone[2], Paola Rossi[6], Ferdinando Rossi[4], Gian Giacomo Consalez[5], Pietro Luigi Poliani[3] and Rossella Galli[1*]

[1]Neural Stem Cell Biology Unit, Division of Regenerative Medicine, Stem Cells & Gene Therapy, San Raffaele Scientific Institute, Via Olgettina 58, Milan, Italy;
[2]Bio))flag, Ltd, Scientific and Technologic Park of Sardinia Polaris, Località Piscinamanna, Pula (Cagliari), Italy;
[3]Department of Pathology, University of Brescia, Spedali Civili of Brescia, P.le Spedali Civili 1, Brescia, Italy;
[4]Neuroscience Institute of Turin (NIT), Department of Neuroscience, University of Turin, I-10125 Turin, Italy and Neuroscience Institute of the Cavalieri-Ottolenghi Foundation (NICO), University of Turin, Regione Gonzole 10, 10043 Orbassano (Turin), Italy;
[5] Division of Neuroscience, San Raffaele Scientific Institute, Via Olgettina 58, Milan, Italy;
[6] Department of Physiology, University of Pavia, Pavia, Italy;
[7] San Raffaele Diabetes Research Institute (HSR-DRI), Division of Immunology, Transplantation and Infectious Disease, San Raffaele Scientific Institute, Milan, Italy;
[8]Telethon Institute for Gene Therapy - Division of Regenerative Medicine, Stem Cells and Gene Therapy, San Raffaele Scientific Institute;
[9]Neuroradiology Unit and CERMAC, San Raffaele Scientific Institute, Via Olgettina 60, Milan, Italy.

[§]: These authors equally contributed to the work.

*To whom correspondence should be addressed.
Rossella Galli
Neural Stem Cell Biology Unit, Division of Regenerative Medicine, Stem Cells and Gene Therapy
San Raffaele Scientific Institute, Via Olgettina 58, 20132 Milan, Italy
phone +39 02 2643 4626
fax +39 02 2643 4621
E-mail: galli.rossella@hsr.it.

Grant Support:
This work was supported by Fondazione Pierfranco and Luisa Mariani for Child Neurology to R.G.

Running title:
Mouse hindbrain NSCs and MB CSCs predict human MB molecular subclasses

Keywords:
Cancer stem cell; postnatal cerebellar stem cell; medulloblastoma; *Ebf; p53*.

Abstract

Medulloblastoma (MB) arises from mutations occurring in stem/progenitor cells located in restricted hindbrain territories. Here we report that the postnatal ventricular zone lining the IV ventricle (IVv) also harbors *bona fide* stem cells that, remarkably, share the same molecular profile with cerebellar white matter-derived NSCs. To identify novel molecular mediators involved in medulloblastomagenesis, we compared these distinct postnatal hindbrain-derived neural stem cell (NSC) populations, which are potentially tumor-initiating, with compound *Ptch/p53* mutant MB cancer stem cells (CSCs) that *in vivo* faithfully phenotype the different variant of human MB. Transcriptome analysis of both hindbrain NSCs and MB CSCs resulted in the generation of well-defined gene signatures, each reminding of a specific human MB molecular subclass. Most interestingly, MB CSCs upregulated developmentally related genes, such as *Ebfs*, which we show to be highly expressed in human MBs and to play a pivotal role in experimental medulloblastomagenesis. These data indicate that gene expression analysis holds great promise not only for understanding functional differences between distinct CSC populations but also for identifying meaningful signatures that stratify patients beyond histopathological staging.

Significance

As the current management of MB is considered unsatisfactory, the functional and molecular comparison between the cell progenitor lineages from which MB is thought to arise and MB cancer stem cells, *i.e.* the cells responsible for tumor initiation, progression and relapse, might lead to the identification of novel potentially relevant mediators of medulloblastomagenesis. Our findings provide a rationale for the exploitation of mouse CSCs as a valuable preclinical model for human MB, both for the definition of CSC-associated gene signatures holding a highly predictive value when tested across human data sets and for the identification of genes to be targeted therapeutically.

Introduction

Medulloblastoma (MB) is the most common malignant brain tumor of childhood. Surgery alone is not sufficient to eradicate this tumor, and both radiotherapy and chemotherapy are considered inefficient treatments, mostly due to the high vulnerability of young patients to anti-mitotic treatments.

The restricted incidence of MB during childhood relates to the specificity of cerebellar ontogeny, which begins early during embryonic development, reaching its final maturation only after birth (1). This delayed maturation results in a prolonged formative postnatal period, characterized by increased susceptibility to tumor formation. Whereas the majority of patients are diagnosed with a MB at a very early age, suggesting that MBs initiate from mutations occurring during embryonic development in hindbrain germinative regions (2, 3), 20% of MB patients are diagnosed in late adolescence or early adulthood, indicating that MB might also arise postnatally.

Interestingly, different subsets of neural precursors have been shown to persist postnatally within the hindbrain and, as such, are potentially involved in medulloblastomagenesis. In the mouse, the best-characterized progenitor population comprises the so-called cerebellum (CB) granule cell progenitors (GCPs) of the external granular layer (EGL), which are characterized by a peak of proliferation at postnatal day (P) 7 followed by progressive decline and exhaustion within the third postnatal week. GCPs proliferate robustly *in vivo* and *in vitro* in response to Sonic Hedgehog (Shh), and their deregulated proliferation postnatally has been causatively implicated in the development of the desmoplastic MB variant, characterized by alterations in the Shh pathway (2). However, GCPs do not satisfy the requirements for stemness, as they are characterized by limited self-renewal and lack of multipotency. On the contrary, the other population of transiently neurogenic progenitors identified within the CB white matter (WM) during the same post-natal window of EGL GCPs does contain *bona fide* neural stem cells (NSCs) (4, 5). In fact, CB WM progenitors can be cultured *in vitro* in the presence of epidermal growth factor (EGF) and fibroblast growth factor-2 (FGF-2) and display typical features of NSCs, such as self-renewal and *in vitro/in vivo* multipotency (6).

Of note, a third subset of hindbrain neural progenitors has been retrieved in proximity of the IV ventricle (IVv), around which the cerebellum proper develops. IVv-derived progenitors are endowed with persistent neurogenic activity *in vivo* throughout adulthood (7, 8). However, the establishment of long-term self-renewing NSC lines from the IV ventricle has never been reported. Recently, oncogenic transformation of progenitors located in the dorsal brainstem, as IVv NSCs are, has been associated with the development of a subtype of the

"classic" MB variant, whose main molecular feature entails the activation of the WNT pathway (3).

Several studies have demonstrated the existence of cancer stem cells (CSCs) in a variety of tumors, including brain tumors. These cells are responsible for tumor growth and maintenance and, being resistant to standard therapies, are probably involved in tumor relapse. Similar to normal NSCs, CSCs can be isolated from brain tumors and long term cultured *in vitro* in the presence of EGF and FGF-2. By this method, putative CSC lines have been established from desmoplastic MBs developing in *Ptch*$^{+/-}$ mice (9), in combination or not with *p53* loss (10). MB CSCs display the essential requirement for a CSC, *i.e.* the capability to generate new tumors, which closely mimic the human disease in terms of *in vivo* growth and phenotype. Notably, the expression of the CSC marker CD15 specifically enriches for MB CSCs (9, 11).

To identify novel molecular determinants to be pursued as diagnostic markers and/or therapeutic targets in MB CSCs, we set out to establish long-term expanding postnatal NSC lines from the IV ventricle as well as from the cerebellar WM and to compare them with MB CSCs, by hypothesizing the existence of a lineage relationship between postnatal cerebellar NSCs and MBs (6). IVv NSCs were capable to differentiate into the three main lineages of the CNS, both *in vivo* and *in vitro,* thus fulfilling the requirements to qualify as *bona fide* NSCs. By applying the same culture conditions to mouse MBs derived from *Ptch*$^{+/-}$ mutants, with or without the concurrent loss of *p53*, we isolated several MB CSC lines, endowed with self-renewal, multipotency and different tumorigenic potential. When subjected to microarray-based gene expression profiling, normal CB WM and IV ventricle-derived SCs as well as MB-derived CSCs were characterized by distinctive gene signatures, which hold predictive potential when tested against human data sets, as previously shown for other stem cell types (12, 13). Most importantly, some of the genes overexpressed in MB CSCs were also expressed in human MB and played a relevant role in the control of medulloblastomagenesis.

Results

Long-term expanding neural stem cells (NSCs) can be isolated from the postnatal ventricular zone (VZ) of the IV ventricle.

The ventricular zone lining the IV ventricle contains mitotically active cells (Fig. 1A), whose proliferation can be reactivated *in vivo* by infusion of mitogens (14). To assess whether IV ventricle (IVv)-derived NSCs might give rise to long-term expanding NSC lines, we dissected out the IVv region from the hindbrain of C57/B6 mice at post-natal day (P) 7, 14, 21 and 30 (Fig. 1B) and cultured it according to the NeuroSphere Assay (NSA). CB WM and the SVZ lining the two lateral ventricles of the forebrain were used as controls.

At P14, P21 and P30, lines could be generated only from IVv and SVZ, confirming that sustained proliferation of CB WM cells ceased by the first post-natal week (5). Conversely, at P7, long-term expanding cell lines could be established from all the three regions; thus, we analyzed NSCs at this time point.

Cells were isolated from *wt*, *Ptch*$^{+/-}$*p53*$^{+/+}$ and *Ptch*$^{+/-}$*p53*$^{+/-}$ mice. Primary neurosphere formation was observed in all three regions, with SVZ giving rise to a much higher frequency of primary neurospheres than cells from CB and IVv, independent from genotype (Fig. 1B). All the three different region-specific cell cultures contained putative NSCs, which gave rise to clonal NSC lines that self-renewed up to 40 sub-culturing passages *in vitro,* again independent from genotype and, also, from the region of origin (Fig. 1B).

Next, we tested the expression of the NSC markers CD133-Prom1 and CD15/SSEA1 in the three regions and in the clonal NSC lines derived from them. CD15/SSEA1-IR cells were more frequent than CD133/Prom1 cells in every region and in the corresponding NSCs (Fig. 1C). All NSC populations gave rise to neurons, astrocytes and oligodendrocytes, thus demonstrating full multipotency (Fig. 1D and Table S1A). Tuj1-IR cells expressing calbindin and parvalbumin, as well as GABA and glutamate, were retrieved at similar frequencies in the progeny obtained from the three distinct NSC types (data not shown). However, electrophysiological analysis of terminally differentiated neurons obtained from region-specific NSCs indicated that they were intrinsically different in their electroresponsiveness (Fig. 1E). In fact, CB WM and IVv NSC-derived neurons were characterized by inward fast Na^+ and slow Ca^{2+} currents and outward inactivating K^+ current, normally retrieved in functionally mature neurons. On the contrary, most neurons obtained from SVZ NSCs displayed K^+ steady-state currents, typical of immature neuronal cells (Fig. 1E and Table S1B).

To formally prove the stem cell nature of IVv NSCs, GFP-labelled clonal IVv NSCs were transplanted into the cerebellum of neonatal mice (Fig. 1F). Similar to CB WM NSCs, IVv NSCs differentiated into astrocytes,

neuron-like cells and oligodendrocytes. However, IVv NSCs gave rise to a higher frequency of neuron-like cells than CB WM NSCs. Both NSC types dispersed throughout the distinct layers of the CB, namely the EGL, the molecular layer (ML), the internal granular layer (IGL), the WM and the deep cerebellar nuclei (DCN) (Table S1C).

Thus, by demonstrating extensive self-renewal ability and *in vitro/in vivo* multipotency, IVv cells did qualify as *bona fide* NSCs and, together with CB WM NSCs, revealed intrinsic regional characteristics, in terms of *in vitro* and *in vivo* differentiation potential.

Hindbrain- and forebrain-derived NSCs are molecularly distinct.

To assess whether postnatal IVv, CB WM, and SVZ NSCs were also molecularly different, we subjected *wt* and *Ptch*$^{+/-}$*p53*$^{+/+}$ NSCs isolated from the three different regions to whole genome transcriptome analysis at sub-culturing passages comprised between 10 and 15. Notably, *wt* and *Ptch*$^{+/-}$*p53*$^{+/+}$ NSCs clustered together, with no genes resulting differentially expressed between the two cell populations, thus suggesting that *Ptch* heterozygosity did not influence global transcriptome of NSCs (not shown). Gene profiles of hindbrain-derived CB WM and IVv NSCs were sharply distinguishable from that of SVZ NSCs, with 562 differentially expressed probe sets (Fig. 2A and List S1). Overall, gene expression in the distinct NSCs was reminiscent of the pattern of expression observed *in vivo* in the different regions of origin. In fact, forebrain-restricted transcription factors, such as *Emx2* and *FoxG1,* were overexpressed in SVZ NSCs; by contrast, transcription factors normally involved in hindbrain development, such as *En2* and *Pax3*, were upregulated in CB WM and IVv NSCs (Fig. 2B). These *in silico* data were validated in cultured NSCs (Fig. 2B, C) and, most relevantly, in tissue sections comprising the regions of origin (Fig. 2D, E). Thus, region-specific *in vitro* cultured NSCs maintained their *in vivo* regionalization and their positional identity. Remarkably, NSCs isolated from the IVv, *i.e.* an extra-cerebellar region, were molecularly identical to CB WM-derived NSCs.

A lineage relationship between postnatal CB/IVv NSCs and MBs can be hypothesized, as many MBs arise postnatally. To assess whether P7 CB/IVv NSCs may act as MB cell-of-origin when challenged by pro-oncogenic stimuli, we exploited the same experimental strategy by which adult SVZ-derived NSCs, when co-transplanted under the renal capsule with pancreatic islets, were shown to give rise to neuroblastoma-like lesions, as a consequence of sustained insulin-mediated stimulation (15). To this end, we transplanted C57BL/6 mice with syngeneic pancreatic islets and syngeneic GFP-expressing CB/IVv NSCs under the left kidney capsule and with syngeneic GFP NSCs alone under the right kidney capsule. Tumor formation was observed 60

days after transplantation of both GFP CB and IVv NSCs at the site of islets/NSC transplantation (Fig. 2F). The lesions were GFP-IR. Notably, the presence of rosette-like structures suggested that CB/IVv NSC-derived lesions were reminiscent of typical of medulloblastoma/PNET, in line with previous studies in which tumor suppressor-deleted P7 CB NSCs were demonstrated to be tumorigenic (6).

To investigate whether the gene signatures distinguishing hindbrain- *vs.* forebrain-derived NSCs was enriched in molecular subtypes of human MB, after human homologue conversion, we selected 155 genes that were enriched at least 2-fold in hindbrain NSCs vs forebrain NSCs and 142 genes that were enriched at least 2-fold in the reciprocal comparison. Then, we performed Gene Set Enrichment Analysis (GSEA) on a publicly available data set (GSE21140), which contained expression data concerning 103 human MB samples (16). Based on this study, 4 different MB molecular subgroups were identified, namely the Shh group, the WNT group, and groups C and D. Interestingly, the expression of genes upregulated in CB/IVv NSCs was more strongly associated with the desmoplastic MB subgroup than the SVZ gene signature (Fig. 2G, Table S2 and List S1). Accordingly, the same gene signature was exclusively upregulated in the Shh molecular subgroup, which comprise many desmoplastic MBs. As a control, the global 297-gene signature was tested against all the subgroups simultaneously and, again, it sharply separated the Shh phenotype from the others (Fig. S1).

Hindbrain- and forebrain-derived NSCs are Sonic Hedgehog (Shh) pathway-independent.

To assess whether Shh signalling pathway, normally active in GCPs, might be operating also in CB WM and IVv NSCs, we took advantage of the genetic configuration of the *Ptch* targeting vector, which contains a sequence encoding a nuclear beta-galactosidase (*LacZ*) and the neomycin resistance gene. If CB WM and IVv NSCs did express *Ptch in vitro*, they should have been beta-Gal positive and should have survived neomycin selective treatment. The expression of *Ptch-LacZ* by beta-Gal staining was retrieved in the SVZ, in the EGL, in the WM and in scattered cells around the IVv of P7 $Ptch^{+/-}$ mice *in vivo* (Fig. S2A). When primary cells from the same regions were cultured in the presence of sub-lethal concentration of G418, all the three NSC types were capable to long-term self-renew, thus indicating that CB WM and IVv NSCs did express *Ptch* (not shown). However, when *wt* and $Ptch^{+/-}$ CB WM and IVv NSCs, cultured for more than 6 subculturing passages (SPs), were exposed to 10μM cyclopamine, a Shh pathway inhibitor, no difference in terms of cell survival and proliferation were observed, suggesting that established NSC cultures might grow independent of Shh signaling activation (Fig. S2B). In line with this hypothesis, *Shh* downstream targets were not transcribed in long-term cultured NSC lines, indicating that, in spite of *Ptch* expression, Shh pathway wasn't active and that other

molecular pathways, likely promoted by EGF and FGF2, might be involved in the regulation of NSCs *in vitro* (Fig. S2C, D). To formally prove this concept, we exposed to cyclopamine *wt* and *Ptch*$^{+/-}$ SVZ, CB and IVv NSC lines starting at SP0 (*i.e.* primary culture) up to SP14. Remarkably, a 40% reduction in survival was retrieved in all NSC lines at very early stages of culture in response to Shh pathway inhibition, whereas the same effect was not observed in the same NSCs after additional SPs. (Fig. S2D). Accordingly, overexpression of Shh pathway downstream targets as *Gli1* and *Gli2* as well as marked downregulation of *Gli3* were detected in short-term cultured NSCs, while being absent in long-term cultured NSCs (Fig. S2E).

Cancer stem cell (CSC) lines can be established from *Ptch*$^{+/-}$ mice, independent of p53 loss and Shh pathway activation.

MB tissues were isolated from adult *Ptch*$^{+/-}$*p53*$^{+/+}$, *Ptch*$^{+/-}$ *p53*$^{+/-}$ and *Ptch*$^{+/-}$ *p53*$^{-/-}$ mice and the cell suspensions cultured under the NSA standard conditions (9). Part of each cell suspension was cultured in the presence of serum and in the absence of mitogens, in order to generate serum-dependent cancer cell lines to be exploited as non-stem cell controls (17). After 30-60 DIV, stable CSC lines could be obtained (n=10 from *Ptch*$^{+/-}$*p53*$^{+/+}$ mice, n=4 from *Ptch*$^{+/-}$ *p53*$^{+/-}$ mice, and n=2 from *Ptch*$^{+/-}$ *p53*$^{-/-}$ mice). Some cell lines grew as small clusters similar to neurospheres, while other as adherent cells. MB cells were capable to expand in culture not only in the presence of both EGF and FGF2 (Fig. 3A), but also in the presence of either growth factor alone (data not shown). Importantly, all cell lines expanded for over 100 passages, with the average doubling time comprised between 2 and 5 days. Interestingly, MB CSC lines were heterogeneous in terms of growth rate and clonal efficiency, which was independent from the genotype (Fig. 3A, B). Single MB cells could also give rise to clonal cell lines, identical to their sibling bulk cultures and endowed with the same intrinsic growth properties of their parental cell lines. Similar to normal NSCs, all clonally derived MB cell lines differentiated into Tuj1-IR neuron-like cells, GFAP-positive astrocyte-like cells and NG2/O4-IR oligodendrocyte-like cells, thus proving their multipotency (Fig. 3C and Table S3). Differentiated CSC-derived cultures comprised a variable fraction of cells, which co-labeled with neuronal and glial markers, thus reflecting the activation of an abnormal differentiation program (18) (Table S3). Based on these lines of evidences, MBs derived from *Ptch*$^{+/-}$ mice, independent of *p53* loss, were shown to contain long-term self-renewing and multipotent cells. MB CSCs were able to proliferate and self-maintain in the presence of G418, indicating that *Ptch* transcription was active in these cells (data not shown). To assess whether the Shh signaling pathway was necessary for CSC growth, we exposed different MB CSC lines to cyclopamine (Fig. S3A). Only few of our MB cell lines showed a very

modest decrease in survival upon Shh signaling inhibition. Accordingly, activation of the Shh pathway was lower in MB CSCs than in MB tissues, despite being slightly higher than in cyclopamine-resistant long-term cultured NSCs (Fig. S3B, C). To experimentally test the presumptive Shh independence of MB CSCs for *in vitro* growth, we inhibited the expression of the main Shh pathway effector Smoothened by RNAi and monitored the effect of *Smo* inhibition on MB CSC proliferation and self-renewal. To this end, we generated stable MB CSC lines in which *Smo* was silenced by means of lentiviral-based shRNAs. One out of 4 Mission shRNA clones (clone 493) significantly decreased Smo protein expression (Fig. S3D). Notably, Smo inhibition, and, as such, Shh pathway inactivation, did not significantly affect MB CSC proliferation and survival (Fig. S3D), thus suggesting that MB CSCs might rely on different growth pathways for efficient growth.

Loss of p53 is required for the tumorigenicity of cancer stem cells isolated from Ptch$^{+/-}$ mouse MBs.

Since the majority of *Ptch*$^{+/-}$ tumors lose expression of the *Ptch* wt allele (9), we tested whether our MB cells were also characterized by loss-of-heterozygosity (LOH) for *Ptch* (Fig. 3D). By DNA genotyping, LOH for *Ptch* was detected in all *Ptch*$^{+/-}$ *p53*$^{+/+}$ MB CSCs, due to the deletion of a large fragment of the DNA genomic locus. Conversely, LOH was absent in their tumor of origin and in the tail tissue. Intriguingly, *Ptch* LOH was never observed in *Ptch*$^{+/-}$*p53*$^{+/-}$ and *Ptch*$^{+/-}$*p53*$^{-/-}$ MB CSCs, whereas LOH for *p53* was consistently detected in these same cells (Fig. 3D). Both *Ptch* and *p53* LOH resulted in the absence of the corresponding transcripts (data not shown).

When injected into immuno-suppressed animals, both intracranially (*i.c.*) (striatum and/or cerebellum) and subcutaneously (*s.c.*), either in adult or early post-natal animals, *Ptch*$^{+/-}$ *p53*$^{+/+}$ MB cells gave rise to grafts that were characterized by very slow growth rates and never evolved into full-blown lesions (data not shown). Conversely, *Ptch*$^{+/-}$*p53*$^{+/-}$ and *Ptch*$^{+/-}$*p53*$^{-/-}$ MB cell lines reproducibly established tumors, with a take efficiency of 70% and 100% (*i.c.* and *s.c.,* respectively). Of note, *Ptch* LOH did not influence the tumorigenic potential of MB CSC lines, as all tumorigenic CSC lines retained the expression of the wt *Ptch* allele. Rather, *p53* loss, occurring by genomic deletion or by somatic LOH (Fig. 3D), was strictly required for MB tumorigenesis. Intracranial tumors were detected by MRI after 10-12 weeks after transplantation and fully developed within 30 weeks. Conversely, subcutaneous tumors were observed as early as at 2 weeks after transplantation and progressed very rapidly. Remarkably, only MB CSC lines established *in vitro* by the NSA were capable to generate tumors, while matched serum-dependent non-stem cancer cell lines failed in doing so, even after 150 days from transplantation (not shown).

CSC-derived intracranial tumors resembled spontaneous *Ptch*$^{+/-}$ tumors more closely than subcutaneous tumors, although the histological appearance of CSC-derived intracranial tumors was more malignant and pleomorphic than that of *Ptc* spontaneous tumors, with marked atypia and the presence of infiltrating cellular nests. Indeed, CSC-derived intracranial tumors expressed markers typical of human MB, such as the neuronal markers Tuj1, NeuN, and synaptophysin, as well as the astrocytic marker GFAP (Fig. 3E). Interestingly, in a few circumstances, intracranial tumors escaped the site of implantation, through either leptomeningeal or extracranial dissemination. Tumors infiltrating the meninges resembled intracranial tumors, albeit expressing lower level of neuronal and glial markers, whereas extracranial tumors were highly undifferentiated, with signs of pleomorphism and elevated malignancy. CSC-derived subcutaneous tumors were the most highly undifferentiated, showing a myxoid and heterogeneous morphology, and expressing only Tuj1, while being immunonegative for NeuN and synaptophysin. Thus, the site of tumor formation affects the histological phenotype of experimental CSC-derived MBs, with a progressive malignant evolution from lowly malignant intracranial tumors to highly malignant extra-CNS neoplasias. Accordingly, the frequency of cells expressing the putative CSC marker Sox2 increased from lowly to highly malignant tumors (Fig. 3E).

Molecular analysis of MB CSCs and normal NSCs identified novel potential MB targets.

To identify dysregulated genes that may play a role in the pathogenesis of MB, we first compared the global gene expression profiles of all our MB CSCs with that of normal NSCs. Unsupervised clustering analysis showed that, as expected, MB CSCs shared many more molecular determinants with hindbrain NSCs than with SVZ NSCs, although being clearly distinguishable. In particular, many more genes were differentially expressed between hindbrain NSCs and *Ptch*$^{+/-}$*p53*$^{-/-}$ MB CSCs than between hindbrain NSCs and *Ptch*$^{+/-}$*p53*$^{+/+}$ MB CSCs (Fig. 4A). Accordingly, *Ptch*$^{+/-}$*p53*$^{+/+}$ MB CSCs grouped together and their gene expression profile was different from that of *Ptch*$^{+/-}$ *p53*$^{-/-}$ MB CSCs.

These gene expression data were then exploited to generate gene signatures that reflected the behavior of the distinct populations of MB CSCs (Fig. 4B). The first signature was upregulated exclusively in tumorigenic *Ptch*$^{+/-}$ *p53*$^{-/-}$ MB CSCs vs. hindbrain NSCs (MB1_EXCLUSIVE, 980 genes, List S2), the second exclusively in non-tumorigenic *Ptch*$^{+/-}$ *p53*$^{+/+}$ MB CSCs vs. hindbrain NSCs (MB2_EXCLUSIVE, 105 genes, List S2), and the third comprised the probe sets, whose expression was shared by both tumorigenic and non-tumorigenic CSCs vs. hindbrain NSCs (MB1_MB2 COMMON, 81 genes, List S2). The different gene signatures were validated by testing the expression of randomly selected transcripts on independent RNA preparations of the

corresponding samples, with 90% concordance with the GeneChip data (not shown). We investigated whether the different gene signatures could stratify MBs according to their molecular characteristics, as exemplified by their enrichment in specific molecular subclasses (Fig. 4B and Table S4). The MB1_EXCLUSIVE and MB1_MB2 COMMON gene signatures were specifically enriched in the desmoplastic subgroup. However, MB1_MB2 COMMON gene signature was associated with the Shh molecular subgroup, while MB1_EXCLUSIVE was enriched in the WNT molecular subgroup. To validate the *in silico*-determined expression of WNT pathway mediators in the gene signature associated with *Ptch*$^{+/-}$ *p53*$^{-/-}$ MB CSCs (MB1_EXCLUSIVE), we tested the expression of different WNT pathway mediators in the experimental tumors generated from *Ptch*$^{+/-}$ *p53*$^{-/-}$ and *Ptch*$^{+/-}$ *p53*$^{+/+}$ MB CSCs as well as in *Ptch*$^{+/-}$ *p53*$^{-/-}$ and *Ptch*$^{+/-}$ *p53*$^{+/+}$ MB CSC lines (Fig. S5). Interestingly, expression of beta-catenin, the major WNT pathway effector, was retrieved in the cytoplasm of most tumor cells of *Ptch*$^{+/-}$ *p53*$^{+/-}$ spontaneous tumors and *Ptch*$^{+/-}$ *p53*$^{-/-}$ MB CSC-derived intracranial and subcutaneous tumors, with nuclear localization of beta-catenin found in about 20% of tumor cells (Fig. S5A). In agreement with GSEA data, beta-catenin protein expression was not detected in *Ptch*$^{+/-}$ *p53*$^{+/+}$spontaneous tumors (Fig. S5A) and in *Ptch*$^{+/-}$ *p53*$^{+/+}$ MB CSC-derived intracranial grafts (not shown). Accordingly, also *in vitro* beta-catenin was expressed only in *Ptch*$^{+/-}$ *p53*$^{-/-}$ MB CSCs (Fig. S5B). In line with beta-catenin expression, transcripts for 6 WNT pathway mediators included in the MB1_EXCLUSIVE gene signature, such as *Lef*, *Tcf3*, *Bcat1*, *Fzd6*, *Wif1* and *Kremen1,* were significantly upregulated in *Ptch*$^{+/-}$ *p53*$^{-/-}$ MB CSC lines as compared to *Ptch*$^{+/-}$ *p53*$^{+/+}$ MB CSCs (Fig. S5C). Notably, when the same gene signatures were tested against all the human MB subgroups, they segregated the same subgroups as indicated by GSEA (Fig. S4). Thus, human MBs can be distinguished based on their degree of resemblance to distinct mouse MB CSC molecular phenotypes.

Reactivation of developmentally regulated molecular programs promotes medulloblastomagenesis.

Several DEGs, which were upregulated in MB CSCs, were also expressed in the cerebellum during embryonic development, thus suggesting that they could play both physiological and pro-oncogenic functions. In particular, we focused on Hedgehog interacting protein (*Hhip*) and early B-cell factors (*Ebfs*).

Hhip was upregulated selectively in *Ptch*$^{+/-}$ *p53*$^{+/+}$ MB CSCs (List S2) and its expression was retrieved both at the transcriptional and protein level in CSC-derived tumors and in *Ptc* spontaneous tumors (Fig. S6A). From *in silico* analysis, *HHIP* was selectively expressed in human desmoplastic MBs, while being absent in classic MBs (Fig. S6B, C). Accordingly, expression of HHIP protein was observed only in human desmoplastic MBs, *i.e.* the

histological group molecularly associated to the activation of the Shh pathway (Fig. S6D). Within desmoplastic MBs, HHIP was restricted to desmoplastic areas.

As *Hhip*, Ebf genes, such as *Ebf2* and, in particular, *Ebf3,* were upregulated in MB CSCs and in their corresponding tumor tissues (Fig. 4C). Interestingly, *Ebf3* expression was observed in cycling progenitors located in the EGL as early as at P3, peaked at P7 and decreased around P15. Accordingly, Ebf protein expression was retrieved in EGL progenitors, but also in the prospective WM and around the IVv (Fig. 4E). In line with gene expression data, Ebf-IR cells were retrieved at very high frequency in both spontaneous $Ptch^{+/-}$ and experimental intracranial CSC-derived tumors, while being rare in intrameningeal and subcutaneous CSC-derived tumors (Fig. 4E).

EBF3 expression *in silico* was retrieved in human MB samples and in a small fraction of neuroblastomas, suggesting a possible correlation between the expression of the gene and the phenotype of neuronal tumors (Fig. S5A, B). Selective expression of *EBF3* in human MBs was retrieved by qPCR in human MBs, while being absent in glioblastomas multiforme (GBMs) (Fig. 4F), *i.e.* tumors characterized by glial differentiation, in which *EBF3* expression is epigenetically silenced. EBF protein expression was also tested on a series of 33 MB post-surgery specimens and in GBM as controls (Fig. 4G and Table S5). In agreement with transcriptional data, EBF proteins were retrieved in all MBs, but not in GBMs (not shown). The pattern of expression of the EBF proteins varied among histological variants of MB. In particular, classic MB displayed intense EBF staining in the majority of tumor cells, whereas desmoplastic MBs were characterized by EBF expression being restricted to desmoplastic portions of the tumor and excluded from the nodular part. Of note, EBF proteins were also strongly expressed in pleomorphic giant cells found in large cell anaplastic MBs.

To start addressing the putative role of *Ebf3* in the regulation of normal NSCs and MB CSCs, we transduced both NSC and CSC lines with a lentiviral vector coding for *Ebf3* full-length cDNA, featuring the FLAG epitope as a tag (Fig. 5A), obtaining efficient expression of both *Ebf3* transcript (Fig. 5A) and protein (Fig. 5B). Mock- and *Ebf3*-tranduced NSC and CSC lines did not show any difference in proliferation, long-term self-renewal, migration and apoptosis (not shown). However, when maintained under proliferative culture conditions (*i.e.* in the presence of EGF and FGF2), *Ebf3*-transduced NSC and CSC lines acquired the appearance of cells undergoing differentiation. To validate this observation, we assessed the expression of differentiation markers (Fig. 5C). While normal mock-transduced IVv, CB and SVZ NSCs were almost negative for lineage differentiation markers, *Ebf3*-overexpressing NSCs showed a consistent increase in the frequency of FLAG-positive cells expressing the neuronal marker Tuj1 and displaying a mature cellular morphology (Fig. 5C and

S7). Likewise, *Ebf3*-overexpressing FLAG-positive CSCs did give rise to Tuj1-IR cells displaying a more mature morphology than Tuj1-IR cells in mock-transduced CSC cultures (Fig. 5C). The frequency of astrocytes and oligodendrocytes cells was similar between mock- and *Ebf3*-transduced NSC/CSCs (not shown). Of note, the same enhanced cell differentiation observed under proliferative conditions upon *Ebf3* over-expression was even more evident when NSCs and CSCs were challenged to differentiate (Fig. 5D). *Ebf3*-overexpressing cultures mostly generated FLAG-positive cells neuronal-like cells, featuring extended processes and well-developed neurites (Fig. 5D). Notably, putative *Ebf* transcriptional targets such as p21, p27 and p57 were expressed at the same level in mock- and *Ebf3*-overexpressing NSCs/CSCs (not shown).

To test whether *Ebf3* over-expression affected the tumorigenic potential of MB CSCs, mock- and *Ebf3*-transduced CSC lines were transplanted intracranially into adult immuno-deficient mice. Surprisingly, in spite of very high *Ebf3* overexpression efficiency as shown by FLAG staining (Fig. 6A), no significant differences in the tumorigenic ability of *Ebf3*-overexpressing CSCs were observed with respect to mock-transduced CSCs. However, the frequency of cells endogenously expressing Ebf in mock CSC-derived intracranial tumors was very high and comparable to that in *Ebf3*-expressing tumors. Therefore, *Ebf3* overexpression in CSCs under intracranial transplantation settings wasn't functionally relevant.

To overcome this limitation, we set out to inject mock- and *Ebf3*-tranduced CSC lines subcutaneously, as under this transplantation setting basal Ebf expression in mock CSC-derived tumors was low (Fig. 4E). In fact, mock CSC-derived *s.c.* tumors were immunoreactive for GFP and mildly positive for Ebf, whereas *Ebf3*-overexpressing tumors were immunoreactive for FLAG and strongly positive for Ebf (Fig. 6B). Upon subcutaneous transplantation, *Ebf3*-overexpressing tumors grew more rapidly than those generated by mock-transduced cells (Fig. 6C) and this was also reflected in the histological appearance of tumors (Fig. 6D). Indeed, whereas mock CSC-derived tumors were characterized by sarcomatoid/myxoid morphology and by the presence of spindle-shaped cells, *Ebf3*-tranduced CSC-derived tumors were more highly undifferentiated, with a pleomorphic and malignant appearance and the presence of perivascular cellular rosettes and necrosis. Likewise, whereas mock tumors did contain Tuj1- and GFAP-IR cells, *Ebf3*-transduced CSC-derived tumors comprised only Tuj1-IR cells. Overall, whereas subcutaneous mock tumors did remind of classic MBs, *Ebf3*-overexpressing tumors resembled highly malignant PNET-like anaplastic MBs. In line with these findings, both the mitotic index by Ki67 and the frequency of Sox2-IR cells were significantly higher in *Ebf3*-tranduced CSC-derived tumors than in mock CSC-derived tumors (Fig. 6E). To be noted, the expression of *Ebfs* downstream targets p21, p27 and p57, which are known to restrain tumor growth, was higher in *Ebf3*-overexpressing CSC-

derived tumors than in mock CSC-derived tumors, suggesting that their activation in this cellular context might be part of an inefficient rebound compensatory mechanism activated by *Ebf3*-expressing cells to limit tumor proliferation (Fig. S8).

To test whether *Ebf3* overexpression *per se* might promote transformation and/or tumor-initiation, we transduced hindbrain-derived NSCs as well as lowly tumorigenic $Ptch^{+/-}$ $p53^{+/+}$ MB CSCs with *Ebf3*-coding vectors and implanted them *s.c.* into nude mice. After 120 days from transplantation, no sign of tumor development was detected in mice injected with either type of *Ebf3*-overexpressing cell line (not shown).

Finally, to formally address the role of *Ebf3* in CSCs under physiological conditions, we set out to inhibit *Ebf3* endogenous expression in MB CSCs by RNAi. Given that *Ebf* family members function as active heterodimers, we took advantage of a GFP-coding retroviral construct that allows the concomitant expression of siRNAs against *Ebf1*-, *Ebf2*-, and *Ebf3* (19). After transduction, significant down-regulation of *Ebf2* and *Ebf3* transcripts was observed in *Ebf*-silenced MB CSCs (Fig. 6F). Accordingly, 60% decrease in Ebf3 protein expression was detected in the same cells (Fig. 6F). Then, we examined the effect of siRNA-mediated downregulation of Ebf3 protein expression on the tumorigenic potential of MB CSCs. To this end, we transplanted mock- and *Ebf*-silenced MB CSCs subcutaneously. Sixty days after transplantation, *Ebf*-silenced tumors were significantly smaller than those generated by mock-transduced cells (Fig. 6G) and, again, this defect was reflected in the histological appearance of tumors (Fig. 6G). In fact, whereas mock CSC-derived tumors showed the typical sarcomatoid/myxoid morphology, tumors in which *Ebf3* was silenced were characterized by a homogeneous, well-differentiated morphology and reduced proliferation, with cells displaying large and eosinophil cytoplasm, suggestive of a less malignant phenotype.

Discussion

In order to identify novel molecular targets involved in MB tumorigenesis to be exploited for selective and effective therapies, we took advantage of the strict biological relationship existing between the tumor and the cell progenitor lineages from which MB is thought to arise. In fact, different clinical/molecular MB subtypes are believed to originate from mutations occurring in distinct stem/precursor cells located in cerebellar germinative regions, such as the rhombic lip derivative and the ventricular zone (VZ) matrix (20), as well as in extra-cerebellar domains, as the dorsal brainstem (3), some of them persisting postnatally (2).

Neural stem cells (NSCs) can be isolated from extracerebellar anatomical sites as the IV ventricle and share functional and molecular features with cerebellar NSCs.

During embryonic development, two primary cerebellar neurogenic epithelia, *i.e.* the rhombic lip (RL) and the IV ventricle ventricular zone (VZ), segregate as early as at embryonic day 9 (E9) and represent the birthplace of all GABAergic and glutamatergic lineages, respectively (1, 21). Early post-natally, the RL derivative located at the cerebellar surface, *i.e.* the external granular layer (EGL), undergoes a massive expansion due to granule cell precursor (GCP) proliferation that peaks at around P7 and gradually ceases, being completely exhausted within the third post-natal week in rodents and the first year in humans (22). Very recently, a second postnatal cerebellar neurogenic compartment has been identified within the cerebellar WM (4, 5). Putative CB WM NSCs demonstrated to self-renew shortly in culture and to give rise to neurons, astrocytes and oligodendrocytes both *in vitro* and *in vivo* (4). When compared to forebrain embryonic stem cells, they maintained regional characteristics, as the antigenic phenotype of the cells they generated upon transplantation was reminiscent of the NSC region of origin. The same CB WM NSCs were characterized as being Math1^{neg}/lineage^{neg}/prominin^{pos} cells and are uniquely responsible for neurosphere generation in culture (5). In agreement with these findings, we generated P7 CB WM neurospheres, which were subcultured for many passages, giving rise to long term expanding NSCs (6). Most interestingly, by applying the same culture conditions to cells obtained from the P7 brain parenchyma surrounding the IV ventricle, from which short-term proliferating precursors were previously isolated (7, 8), we established long term self-renewing multipotent *bona fide* IVv NSCs.

As previously shown for NSCs isolated from different embryonic brain regions (23), the distinct postnatal NSC populations did maintain their original positional identity. In fact, both CB and IVv NSCs overexpressed transcription factors, such as *Pax3* and *En2,* which are well known regulators of hindbrain development.

Likewise, SVZ NSCs displayed enhanced expression of genes involved in forebrain development, *e.g. Emx2*, *Foxg1*, and *Lhx2*. Most interestingly, IVv NSCs, which were isolated from an extra-cerebellar region, were molecularly indistinguishable from CB WM NSCs, thus suggesting that progenitors residing in different anatomical sites might have a common origin. Relevantly, when appropriately challenged, hindbrain-derived NSCs generate medulloblastoma/PNET-like lesions, thus reinforcing the notion that multiple populations of hindbrain NSCs may be at the origin of MB (3). Notably, IVv NSCs could be isolated not only from early postnatal mice but also from adults, well correlating with the observation that MBs deriving from brainstem progenitors show a distributed age of onset, ranging from late infancy to adulthood, with a peak in older children (24).

Molecular analysis of MB-derived CSC and hindbrain-derived NSCs identifies potential molecular mediators of medulloblastomagenesis.

In agreement with previous observations in MB cultures and serum-cultured colon cancer cells (25, 26), the expression of downstream mediators of Shh pathway in NSCs and MB CSCs was modest, and, accordingly, Shh pathway activation was only marginally relevant for the proliferation and self-renewal of NSC/CSCs *in vitro*. Indeed, we demonstrated that addiction to Shh pathway occurs in NSCs only at early subculturing passages, when Shh pathway is still active. Accordingly, Shh inhibition in long-term cultured MB CSCs by Smo RNAi does not influence CSC proliferation. Strikingly, in spite of the overall scarce activation of Shh pathway in both long-term NSC/CSCs, *Hhip* was upregulated significantly in $Ptch^{+/-}p53^{+/+}$ MB CSCs. As *Hhip* acts as a sort of "decoy" receptor for Shh, its persistent expression *in vitro* in $Ptch^{+/-}p53^{+/+}$ MB CSCs, which lack expression of the *wt* allele for *Ptch* by LOH, might be the result of compensatory transcriptional regulatory loops.

These results are in contrast with many reports that documented full activation of Shh pathway in normal NSCs (27) as well as in CSCs isolated from the same *Ptch* mouse model (28) or other brain tumors (29). One possible explanation relies in the fact that both NSC/CSC-derived neurospheres employed in those studies were maintained *in vitro* for very few subculturing passages. As such, short-term NSC/CSC cultures, which are mostly composed by committed progenitors (30), might have been addicted to Shh signaling and, therefore, responded to Shh inhibition by reduced survival and proliferation. On the contrary, long-term propagated cultures, which are highly enriched in the NSC/CSC component and devoid of lineage-restricted precursors (30), might not be Shh-dependent and may self-maintain through different signaling pathways. In fact, Shh alone is unable to sustain SVZ neurosphere growth *in vitro* and addition of Shh to neurosphere media containing

saturating doses of EGF is ineffective in increasing the number of neurospheres generated (27), suggesting that Shh pathway might act more as a relevant co-factor rather than as an indispensable mediator of NSC proliferation/self-renewal in culture. Alternatively, chronic exposure of NSC/CSCs to mitogenic stimulation, in particular to FGF2 (31), might repress Shh pathway activation and promote the activity of different compensatory effectors. Further studies will help dissecting the mechanism(s) underlying hedgehog pathway regulation in EGF/FGF2-established NSC/CSC lines.

Notably, although Shh pathway activation was not retrieved in postnatal NSCs, the CB/IVv NSC gene signature is significantly associated with the Shh human molecular subgroup, suggesting that modifications in Shh pathway might be the primary mutational event responsible for MB initiation. At the same time, this observation proposes CB IV and IVv NSCs as additional cells-of-origin for MBs, as they share the activation of the Shh pathway with EGL GCPs, which are well know to be causatively involved in MB tumorigenesis (32, 33).

Interestingly, the genes characterizing *Ptch* heterozygous MB CSCs were associated with the Shh molecular subgroup of human MBs, thus emphasizing the exploitability of $Ptch^{+/-}p53^{+/+}$ MB CSCs as an *in vitro* pre-clinical model of Shh-dependent MB. Likewise, the highly tumorigenic $Ptch^{+/-}p53^{-/-}$ MB CSCs, whose gene signature is highly enriched in the WNT subgroup, might be used for modeling this subtype of MB, both *in vivo* and *in vitro*. Along this line, the observation that the site of transplantation of MB CSCs under experimental *in vivo* settings results in tumors endowed with varying degree of malignancy, ranging from desmoplastic well-differentiated intracranial tumors to highly undifferentiated anaplastic subcutaneous tumors, further underline the relevance of MB CSCs as a versatile model, highly representative of the different variant of human MBs.

In line with a recent report (9), we established long-term self-renewing CSC lines from MBs, which spontaneously develop in *Ptch* heterozygous mice (34) and in compound *Ptch/p53* mutants (10). However, only MB CSCs, characterized by genetic or somatic p53 loss, as we reported in this study, were able to generate fully developed experimental tumors, which closely mimic the different histological variants of the human disease. Thus, loss of p53 is an obligated step for CSC-initiated medulloblastomagenesis to occur (3). Interestingly, the gene signature distinguishing $Ptch^{+/-}p53^{-/-}$ MB CSCs is enriched in the WNT subgroup, in agreement with the recent finding that, in MB patients, *p53* mutations are mostly found in favorable-risk WNT-subtype MBs (35).

Most notably, by molecularly comparing MB CSCs and hindbrain NSCs, we pinpointed candidate molecular markers, potentially exploitable as MB prognostic-diagnostic markers. *HHIP* was detected in human MBs, associated to the MB desmoplastic variant, while being low or absent in human classic/anaplastic MBs by

epigenetic silencing (36). *Hhip* competes with *Ptch* receptor for Hh binding and its expression is induced by ectopic activation of Hedgehog signaling (37, 38). Notably, *Hhip* is overexpressed in CD133 positive colon CSCs (39). Accordingly, HHIP is highly expressed in the subgroup of human MBs activating the Shh pathway, *i.e.* the group more closely associated to the desmoplastic variant, thus supporting the strict correlation between *Hhip* expression and desmoplastic MBs (24).

Reactivation of developmentally regulated proneural molecular programs favors medulloblastomagenesis

During development, *Ebf* transcription factors are expressed within the region extending from midbrain to spinal cord, being selectively expressed in early post-mitotic neurons (40). However, we observed that *Ebf3* expression was retrieved not only in postmitotic GCPs of the inner EGL, but also in BrdU-incorporating GCPs undergoing neuronal fate choice in the outer EGL. Accordingly, enforced expression of *Ebf3* in NSCs and MB CSCs did not induce cell cycle arrest or apoptosis, but, rather, premature and enhanced neuronal commitment, which was already evident under proliferative conditions and was maintained upon differentiation.

Most interestingly, enforced expression of *Ebf3* in MB CSCs greatly increased their tumorigenic ability, indicating that the *Ebf3*-mediated induction of a neuronal phenotype in MB cells might be required to promote MB initiation and progression, in line with recent reports proposing that the acquisition of granule cell neuronal commitment is essential for medulloblastomagenesis (32, 33). Of note, the molecular subgroup of human MBs showing a highly malignant behavior is associated with a neuronal signature (24).

Ebf3 expression is known to be absent in many human cancers, including leukemias, pancreatic cancers, head and neck squamous cell carcinomas and, most interestingly, glioblastomas multiforme (GBMs). In many of these cancers, EBF3 inactivation is due to epigenetic silencing by promoter methylation, genomic deletion or point mutations. As expected, *Ebf*3 expression in these tumor cells induces cell cycle arrest and apoptosis, indicating that *Ebf3* could act as tumor suppressor (41). By contrast, our findings suggest that *Ebf3* expression in malignancies belonging to the neuronal lineage, such as MBs and, possibly, neuroblastomas, might play a pro-oncogenic role, in contrast with glial tumors and other cancers.

Legends

Figure 1 - Long-term expanding neural stem cells can be isolated from the post-natal IV ventricle region.

(A) Expression of PH3, Ki67 and BrdU in CB EGL and WM, IV ventricle and SVZ at P7. Magnification 200x. (B) CB WM and the region lining the IV ventricle were dissected as described in the drawing (upper left panel). For IV ventricle cultures, only the floor of the ventricle was included. Clonal efficiency in hindbrain- and SVZ-derived primary cell cultures (upper right panel; *** p= 0.0001; **** p< 0.0001). Long-term growth curves (lower left panel) and clonogenic assay (lower right panel) of NSC lines. (C) Stem cell marker expression in the different neurogenic regions (left panels), after exclusion of $CD45^+$ stromal cells, and in their corresponding NSC lines (right panels). (D) Multipotency of CB, IVv and SVZ NSCs (Tuj1-IR neurons, green; GFAP-IR astrocytes, red; NG2-IR oligodendroglial progenitors, red; O4-IR oligodendrocytes, green; 600x). (E) Electrophysiological profile of CB, IVv and SVZ NSC-derived neurons. (F) GFP-transduced, hindbrain NSCs after injection into the neonatal cerebellum (S100-IR astroglial cells and Olig2-IR oligodendrocytes. Neuronal-like cells were identified based on cellular morphology). GL, granule layer; ML, molecular layer (600x).

Figure 2 – Molecular comparison of hindbrain-derived NSCs with and forebrain-derived NSCs indicates that regional identity is maintained.

(A) Unsupervised whole-transcript expression analysis of region specific NSC lines. (B) Heatmap highlighting a selection of region-specific DEGs. Validation of the expression of DEGs by semi-quantitative (right panel) and quantitative RT-PCR (lower panels). Fold increase in *Emx2* expression in SVZ NSCs was obtained with respect to CB NSCs; fold increase in *Pax3* expression in CB and IVv NSCs was calculated with respect to SVZ NSCs. (C) Pax3 protein nuclear expression in CB and IVv NSCs (200x). (D) ISH for *En2* and *Emx2* mRNA on P7 brain tissue (200x). (E) IHC for Pax3 and FoxG1 (400x). (F) Medulloblastoma/PNET-like lesions are generated by the co-implantation of GFP-labeled CB/IV NSCs with pancreatic islets under the renal capsule. H&E shows the extent of tumor development from CB NSCs (asterisk, 40x, 100x; upper panels). The tumor is GFP-IR (lower left panel). High-magnification fields depict typical rosette-like structures (lower right panel, 200x and 400x). Arrows point to grafted pancreatic islets. (G) GSEA enrichment plots. Each gene signature was compared with molecular subgroups from a human MB data set. The nominal p value and the false discovery rate (FDR) q-value are indicated below.

Figure 3 - Cancer stem cells (CSCs) can be isolated from mouse MBs derived from Ptch$^{+/-}$ mice and give rise to phenotypically distinct experimental tumors.

(A) Growth curves and (B) clonogenic assays of MB CSC lines. (C) MB CSC differentiation into Tuj1-IR neuron-like cells (green), GFAP-IR astrocyte-like cells (red), NG2-IR oligodendrocyte precursors (red) and O4-IR (green) oligodendrocyte-like cells (400x). (D) LOH of the *Ptch* and *p53* alleles by genomic DNA PCR. (E) IHC characterization of CSC-derived experimental tumors. H&E, 200x; Tuj1, NeuN (GC, tumor-entrapped granule cells), synaptophysin, GFAP and Sox2 staining, 200x.

Figure 4 - Molecular comparison of MB CSCs with normal NSCs pinpoints potential MB targets.

(A) Unsupervised analysis of global gene expression profiles of MB CSCs and NSCs (left panel). Scatter plot of probe sets differentially expressed between MB CSCs and CB/IVv NSCs, between highly malignant *Ptch*$^{+/-}$*p53*$^{-/-}$ CSCs and CB/IVv NSCs and between lowly malignant *Ptch*$^{+/-}$*p53*$^{+/+}$CSCs and CB/IVv NSCs (right panels). DEGs with $|\log2FC| > 1$ are plotted outside the region comprised between the two oblique lines. DEGs with a p-value < 0.05 are red or green-colored. (B) GSEA enrichment plots. Each gene signature was compared with molecular subgroups from a human MB data set. The nominal p value and the false discovery rate (FDR) q-value are indicated below. (C) Semi-quantitative and quantitative RT-PCR for *Ebf2* and *Ebf3* in NSCs, MB CSCs and tissues. WB for Ebf3 in NSCs, MB CSCs, and MB tissues. (D) ISH for *Ebf3* in combination with BrdU incorporation analysis. PCL: Purkinje cell layer. (E) Ebf protein expression in P7 hindbrain (upper panels, 100x and 200x). Ebf-IR cells in Ptc spontaneous tumors, and in intracranial, intrameningeal and subcutaneous CSC-derived tumors (400x). (F) Quantitative Ebf3 mRNA expression in human MB, GBM and healthy brain tissue. (G) Ebf protein expression in human MB specimens (100x and 400x).

Figure 5 - Enforced expression of *Ebf3* in NSCs and MB CSCs results in premature neuronal differentiation.

(A) *Ebf3* mRNA expression in mock- and *Ebf3*-transduced NSCs and CSCs. Fold increase of *Ebf3* mRNA was calculated with respect to matched mock-transduced samples. (B) *Ebf3* protein expression upon lentiviral-mediated gene transfer in NSCs and MB CSCs. (C) Neuronal differentiation of *Ebf3*-transduced NSCs and CSCs under proliferative conditions (FLAG, green; Tuj1, red; 400x, inset 800x). (D) Neuronal differentiation of *Ebf3*-transduced NSCs and CSCs under differentiative conditions (FLAG, green; Tuj1, red; 400x, inset 800x).

Figure 6 - Enforced expression of *Ebf3* in MB CSCs results in enhanced tumorigenesis.

(A) Expression of GFP and FLAG in intracranial tumors generated by mock- and Ebf3-transduced CSCs, respectively (400x). Endogenous Ebf expression in both types of tumors (200x). (B) Expression of GFP and FLAG in subcutaneous tumors generated by mock- and *Ebf3*-transduced CSCs, respectively (200x). Ebf expression in both types of tumors (400x). (C) Quantitative assessment of tumor development after subcutaneous transplantation of *Ebf3*-overexpressing and mock-transduced CSCs. (L51, $p<0.0005$; LB, $p<0.005$). (D) H&E, Tuj1 and GFAP staining in mock- and *Ebf3*-transduced CSC-derived experimental tumors (200x) Inset in H&E: perivascular rosette. (E) The frequency of Ki67 and Sox2-IR cells in *Ebf3*-overexpressing and mock CSC-derived tumors ($p<0.001$). (F) Ebf RNAi in MB CSCs resulted in a significant decrease in Ebf2/Ebf3 transcripts. Ebf3 protein was reduced in *Ebf*-silenced CSCs. (G) Quantitative assessment of tumor development after subcutaneous transplantation of *Ebf*-silenced and mock-transduced CSCs (L21, $p<0.01$). H&E and GFP staining in mock- and *Ebf*-silenced CSC-derived experimental tumors (200x).

Methods

Isolation of neural stem cells (NSCs) and cancer stem cells (CSCs)

Neural stem cell (NSC) cultures were established from the SVZ, the cerebellum and the region surrounding the IV ventricle of P7 mice, whereas CSCs were obtained from tumors developed in 3-6 months-old animals. NSC lines were established from tissues pooled from 4-6 mice, whereas CSC lines from single tumors. NSC and CSC lines were cultured and propagated in standard medium as described in (42).

Differentiation of NSCs and CSCs

NSCs and CSCs were differentiated by withdrawal of mitogens from the culture medium and addition of 2% FBS for 7 days (42) and processed for immunocytochemistry. The lists of the antibodies used are available in the Supplementary Methods' section.

Whole cell patch clamp recording

See Supplementary Methods.

In situ Hybridization

Digoxygenin-labeled riboprobes were transcribed from plasmids coding for *Emx2*, *En2* and *Ebf3* cDNAs. Sixteen µm cryostat sections of P3, P7 and P15 brains were processed as described in Supplementary Methods.

Flow cytometric analysis

Tissues samples and NSC/CSC lines were enzymatically and/or mechanically dissociated to obtain a single cell suspension. Single cells were suspended in PBS/BSA 5mg/ml/EDTA 2 mM pH 8 and incubated on ice for 20 minutes. Specific antibodies were diluted in the same solution and then incubated together with the cells for 30 minutes on ice. The acquisition was performed on BD FACS CANTO™ II (Becton and Dickinson, San Jose, CA) instrument and the analysis was done by FCS express 3.0 software. Antibodies used were: FITC-conjugated CD15 (Becton and Dickinson, San Jose, CA) 1:20; PE-conjugated Prominin-1 (eBioscience, San Diego, CA) 1:50, APC-conjugated CD45 (Becton and Dickinson, San Jose, CA), 1:100, PE-conjugated Ter119 (Becton and Dickinson, San Jose, CA), 1:100.

Immunoblotting

Each sample was homogenized in 10x volume of RIPA lysis buffer. Samples were then diluted in Laemmli's SDS-sample buffer. Proteins were separated by electrophoresis on 8% SDS-PAGE and transferred onto trans-blot nitrocellulose membranes (Amersham). Ponceau staining (Sigma, St. Louis, MO) was performed to confirm that the samples were loaded equally. The primary antibodies/antisera used were: mouse anti-Ebf3 (Abnova, 1:1000), mouse anti-GAPDH (Sigma, St. Louis, MO; 1:10000), goat anti-Smo (Santa Cruz, 1:300).

Gene overexpression and silencing

Mouse *Ebf3* cDNA was cloned into the monocistronic transfer lentiviral vector (LV) pCCL.sin.cPPT.PGK.GFP.WPRE11. GFP was excided and substituted with the FLAG-*Ebf3* cassette. Sister cultures were infected with the same vector coding for GFP, as mock control. NSCs and CSCs were transduced with $1x10^7$ TU/ml of each LV for 16 hours. *Ebf3* silencing was achieved by using retroviral constructs coding for short-hairpin DNA directed against the three *Ebf* genes (19). CSCs were transduced through three round of infection. *Smoothened* silencing was performed by exploiting commercially available lentiviral vectors coding for gene-specific shRNA clones (Mission RNAi, Sigma-Aldrich). Infection of CSCs with shRNAs was performed according to the manufacturer's instructions.

Molecular analysis

Total RNA from all samples was extracted using the RNeasy Mini kit (Qiagen, Chatsworth, CA, USA). One µg of total RNA was reverse-transcribed by using first strand synthesis kit Superscript III RNaseH- Reverse Transcriptase (Invitrogen, Carlsbad, CA) and OligodT primers. All the semi-quantitative RT-PCRs were performed using home-designed specific primers and cDNAs were normalized on ß-actin housekeeping gene. Quantitative real-time PCR was performed by IQ SybrGreen technology (Biorad, Hercules, CA), following manufacturer's instructions. ß-actin was used as housekeeping gene. Mouse- and human-specific *Ebf2* and *Ebf3* primers were employed for qPCR (Qiagen, Sa Bioscience).

Microarray-based gene expression profiling

The subculturing passages at which MB CSCs and NSCs were collected for molecular analysis were comprised between the 8th and 20th. Quality control of hybridization was performed by Image Quality, MAplots, Boxplot

and Density Plot, Array normalization was executed by the RMA and GCRMA algorithms. Divisive clustering algorithms were used to obtain dendrograms, where the biological samples were clustered based on the differentially expressed genes. The hierarchical clustering algorithms employed were: a) distances (euclidian, correlation), b) linkage (complete, single, mcquitty, ward, centroid). The differentially expressed genes (DEGs) were obtained based on: a) t-test moderated empirical Bayes, b) p-value (FDR adjusted 0,05), c) cut-off (1 log2 Fold Change, FC).

NSCs injection into neonatal mice

GFP-labelled clonal CB WM and IVv NSC lines were injected into neonatal cerebella as described in (21).

Evaluation of tumorigenicity

For sub-cutaneous injection, 1-2x10^6 CSCs were resuspendend in 100µl PBS and injected into the right flank of 45-60 days old *nu/nu* female mice. Mice were sacrificed at different time points comprised between 4-12 weeks post-injection, according to the cell line originally injected. For intracranial transplantation, 2x10^5 CSCs were resuspended in DMEM and DNase (Sigma, St. Louis, MO) and delivered into the right striatum or the cerebellum by stereotactic injection through a 5µl Hamilton microsyringe. The following coordinates were used: AV= 0; ML= +2.5mm; DV= -3.5mm from bregma for intrastriatal injections and AV=-3.5; ML=0; DV=2 from interaural line for intracerebellar injections. Animals were sacrificed 2-8 months after transplantation. Transplantation of hindbrain NSCs under the renal capsule was performed as described in (15).

Acknowledgements

We thank Laura Magri and Matteo Zanella for help and assistance with molecular analysis.

References

1. Carletti B, Rossi F. Neurogenesis in the cerebellum. Neuroscientist 2008;14:91-100.

2. Gulino A, Arcella A, Giangaspero F. Pathological and molecular heterogeneity of medulloblastoma. Curr Opin Oncol 2008;20:668-75.

3. Gibson P, Tong Y, Robinson G, et al. Subtypes of medulloblastoma have distinct developmental origins. Nature 2010;468:1095-9.

4. Klein C, Butt SJ, Machold RP, Johnson JE, Fishell G. Cerebellum- and forebrain-derived stem cells possess intrinsic regional character. Development 2005;132:4497-508.

5. Lee A, Kessler JD, Read TA, et al. Isolation of neural stem cells from the postnatal cerebellum. Nat Neurosci 2005;8:723-9.

6. Sutter R, Shakhova O, Bhagat H, et al. Cerebellar stem cells act as medulloblastoma-initiating cells in a mouse model and a neural stem cell signature characterizes a subset of human medulloblastomas. Oncogene 2010;29:1845-56.

7. Weiss S, Dunne C, Hewson J, et al. Multipotent CNS stem cells are present in the adult mammalian spinal cord and ventricular neuroaxis. Journal of Neuroscience 1996;16:7599-609.

8. Golmohammadi MG, Blackmore DG, Large B, et al. Comparative analysis of the frequency and distribution of stem and progenitor cells in the adult mouse brain. Stem Cells 2008;26:979-87.

9. Ward RJ, Lee L, Graham K, et al. Multipotent CD15+ cancer stem cells in patched-1-deficient mouse medulloblastoma. Cancer Res 2009;69:4682-90.

10. Wetmore C, Eberhart DE, Curran T. Loss of p53 but not ARF accelerates medulloblastoma in mice heterozygous for patched. Cancer Res 2001;61:513-6.

11. Read TA, Fogarty MP, Markant SL, et al. Identification of CD15 as a marker for tumor-propagating cells in a mouse model of medulloblastoma. Cancer Cell 2009;15:135-47.

12. Pece S, Tosoni D, Confalonieri S, et al. Biological and molecular heterogeneity of breast cancers correlates with their cancer stem cell content. Cell 2010;140:62-73.

13. Merlos-Suarez A, Barriga FM, Jung P, et al. The intestinal stem cell signature identifies colorectal cancer stem cells and predicts disease relapse. Cell Stem Cell 2011;8:511-24.

14. Martens DJ, Seaberg RM, van der Kooy D. In vivo infusions of exogenous growth factors into the fourth ventricle of the adult mouse brain increase the proliferation of neural progenitors around the fourth ventricle and the central canal of the spinal cord. Eur J Neurosci 2002;16:1045-57.

15. Melzi R, Antonioli B, Mercalli A, et al. Co-graft of allogeneic immune regulatory neural stem cells (NPC) and pancreatic islets mediates tolerance, while inducing NPC-derived tumors in mice. PLoS One 2010;5:e10357.

16. Northcott PA, Korshunov A, Witt H, et al. Medulloblastoma Comprises Four Distinct Molecular Variants. J Clin Oncol 2010.

17. Li Z, Bao S, Wu Q, et al. Hypoxia-inducible factors regulate tumorigenic capacity of glioma stem cells. Cancer Cell 2009;15:501-13.

18. Galli R, Binda E, Orfanelli U, et al. Isolation and Characterization of Tumorigenic, Stem-like Neural Precursors from Human Glioblastoma. Cancer Res 2004;64:7011-21.

19. Kieslinger M, Hiechinger S, Dobreva G, Consalez GG, Grosschedl R. Early B cell factor 2 regulates hematopoietic stem cell homeostasis in a cell-nonautonomous manner. Cell Stem Cell 2010;7:496-507.

20. Hatten ME, Roussel MF. Development and cancer of the cerebellum. Trends Neurosci 2011.

21. Leto K, Carletti B, Williams IM, Magrassi L, Rossi F. Different types of cerebellar GABAergic interneurons originate from a common pool of multipotent progenitor cells. J Neurosci 2006;26:11682-94.

22. Wechsler-Reya R, Scott MP. The developmental biology of brain tumors. Annual Review of Neuroscience 2001;24:385-428.

23. Hitoshi S, Tropepe V, Ekker M, van der Kooy D. Neural stem cell lineages are regionally specified, but not committed, within distinct compartments of the developing brain. Development 2002;129:233-44.

24. Kool M, Koster J, Bunt J, et al. Integrated genomics identifies five medulloblastoma subtypes with distinct genetic profiles, pathway signatures and clinicopathological features. PLoS One 2008;3:e3088.

25. Sasai K, Romer JT, Lee Y, et al. Shh pathway activity is down-regulated in cultured medulloblastoma cells: implications for preclinical studies. Cancer Res 2006;66:4215-22.

26. Chatel G, Ganeff C, Boussif N, et al. Hedgehog signaling pathway is inactive in colorectal cancer cell lines. Int J Cancer 2007;121:2622-7.

27. Palma V, Lim DA, Dahmane N, et al. Sonic hedgehog controls stem cell behavior in the postnatal and adult brain. Development 2005;132:335-44.

28. Po A, Ferretti E, Miele E, et al. Hedgehog controls neural stem cells through p53-independent regulation of Nanog. EMBO J 2010;29:2646-58.

29. Zbinden M, Duquet A, Lorente-Trigos A, Ngwabyt SN, Borges I, Ruiz i Altaba A. NANOG regulates glioma stem cells and is essential in vivo acting in a cross-functional network with GLI1 and p53. EMBO J 2010;29:2659-74.

30. Reynolds BA, Rietze RL. Neural stem cells and neurospheres--re-evaluating the relationship. Nat Methods 2005;2:333-6.

31. Fogarty MP, Emmenegger BA, Grasfeder LL, Oliver TG, Wechsler-Reya RJ. Fibroblast growth factor blocks Sonic hedgehog signaling in neuronal precursors and tumor cells. Proc Natl Acad Sci U S A 2007;104:2973-8.

32. Schuller U, Heine VM, Mao J, et al. Acquisition of granule neuron precursor identity is a critical determinant of progenitor cell competence to form Shh-induced medulloblastoma. Cancer Cell 2008;14:123-34.

33. Yang ZJ, Ellis T, Markant SL, et al. Medulloblastoma can be initiated by deletion of Patched in lineage-restricted progenitors or stem cells. Cancer Cell 2008;14:135-45.

34. Goodrich LV, Milenkovic L, Higgins KM, Scott MP. Altered neural cell fates and medulloblastoma in mouse patched mutants. Science 1997;277:1109-13.

35. Pfaff E, Remke M, Sturm D, et al. TP53 mutation is frequently associated with CTNNB1 mutation or MYCN amplification and is compatible with long-term survival in medulloblastoma. J Clin Oncol;28:5188-96.

36. Shahi MH, Afzal M, Sinha S, et al. Human hedgehog interacting protein expression and promoter methylation in medulloblastoma cell lines and primary tumor samples. J Neurooncol 2010;103:287-96.

37. Chuang PT, McMahon AP. Vertebrate Hedgehog signalling modulated by induction of a Hedgehog-binding protein. Nature 1999;397:617-21.

38. Ng JM, Curran T. The Hedgehog's tale: developing strategies for targeting cancer. Nat Rev Cancer 2011;11:493-501.

39. Ruiz i Altaba A. Hedgehog signaling and the Gli code in stem cells, cancer, and metastases. Sci Signal 2011;4:pt9.

40. Garel S, Marin F, Mattei MG, Vesque C, Vincent A, Charnay P. Family of Ebf/Olf-1-related genes potentially involved in neuronal differentiation and regional specification in the central nervous system. Dev Dyn 1997;210:191-205.

41. Zhao LY, Niu Y, Santiago A, et al. An EBF3-mediated transcriptional program that induces cell cycle arrest and apoptosis. Cancer Res 2006;66:9445-52.

42. Galli R, Fiocco R, De Filippis L, et al. Emx2 regulates the proliferation of stem cells of the adult mammalian central nervous system. Development 2002;129:1633-44.

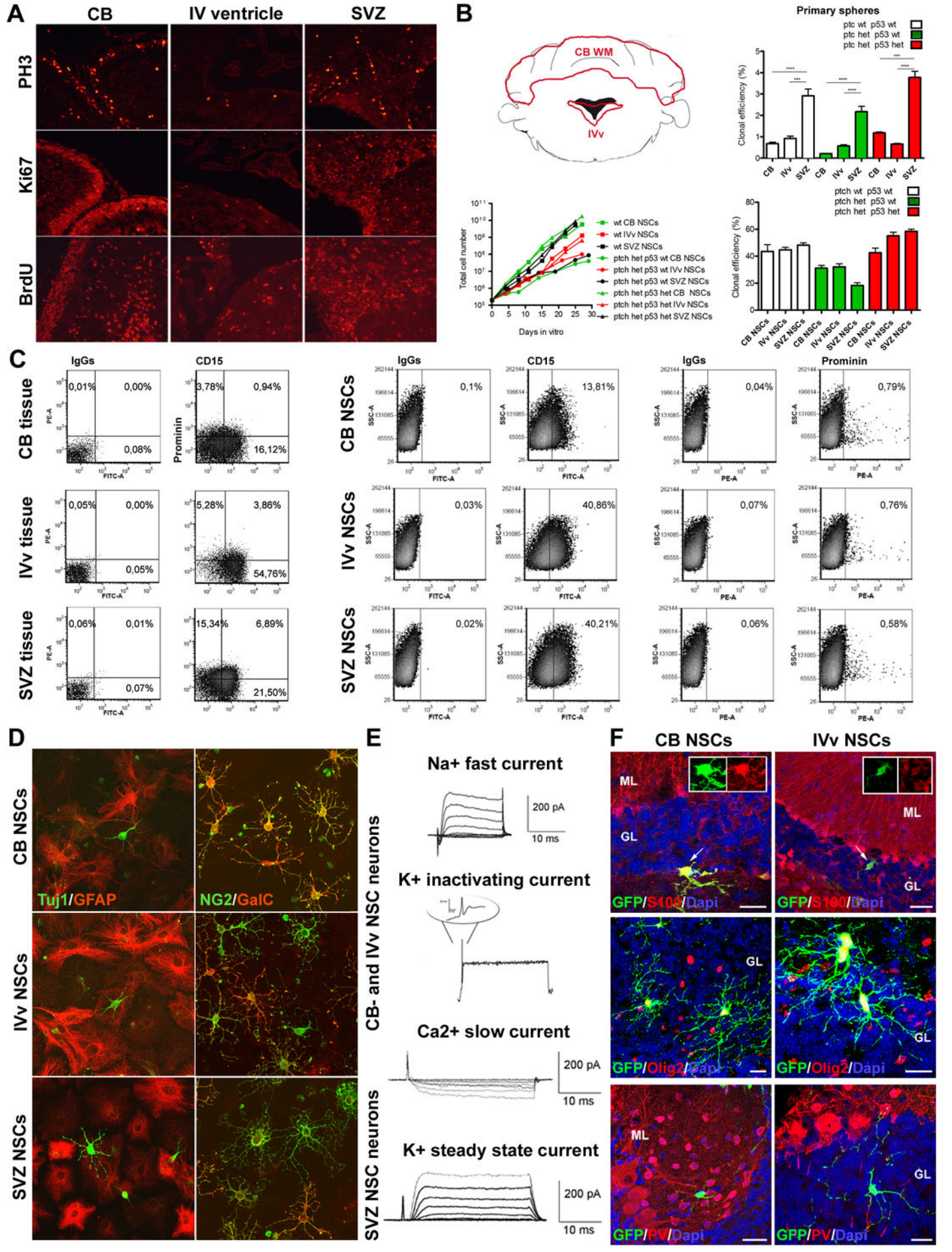
A
CB
IV ventricle
SVZ
PH3
Ki67
BrdU
B
CB WM
IVv
Primary spheres
ptc wt p53 wt
ptc het p53 wt
ptc het p53 het
Clonal efficiency (%)
CB
IVv
SVZ
Total cell number
Days in vitro
wt CB NSCs
wt IVv NSCs
wt SVZ NSCs
ptch het p53 wt CB NSCs
ptch het p53 wt IVv NSCs
ptch het p53 wt SVZ NSCs
ptch het p53 het CB NSCs
ptch het p53 het IVv NSCs
ptch het p53 het SVZ NSCs
ptch wt p53 wt
ptch het p53 wt
ptch het p53 het
CB NSCs
IVv NSCs
SVZ NSCs
C
IgGs
CD15
Prominin
CB tissue
IVv tissue
SVZ tissue
0,01%
0,00%
0,08%
3,78%
0,94%
16,12%
0,05%
0,00%
0,05%
5,28%
3,86%
54,76%
0,06%
0,01%
0,07%
15,34%
6,89%
21,50%
CB NSCs
IVv NSCs
SVZ NSCs
0,1%
13,81%
0,04%
0,79%
0,03%
40,86%
0,07%
0,76%
0,02%
40,21%
0,06%
0,58%
FITC-A
PE-A
SSC-A
D
CB NSCs
IVv NSCs
SVZ NSCs
Tuj1/GFAP
NG2/GalC
E
Na+ fast current
200 pA
10 ms
K+ inactivating current
Ca2+ slow current
K+ steady state current
CB- and IVv NSC neurons
SVZ NSC neurons
F
CB NSCs
IVv NSCs
ML
GL
GFP/S100/Dapi
GFP/Olig2/Dapi
GFP/PV/Dapi

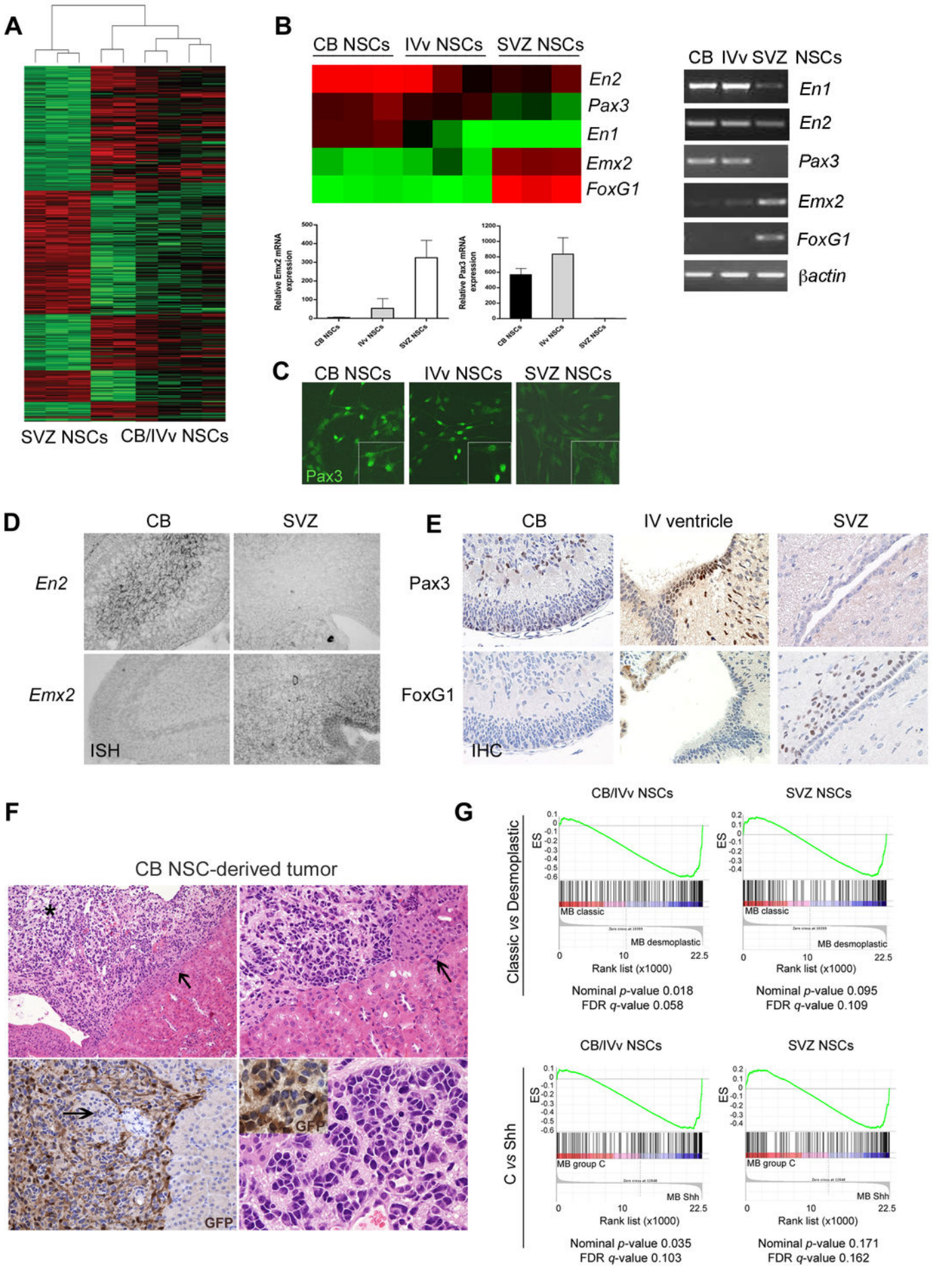
A
SVZ NSCs
CB/IVv NSCs
B
CB NSCs
IVv NSCs
SVZ NSCs
En2
Pax3
En1
Emx2
FoxG1
Relative Emx2 mRNA expression
Relative Pax3 mRNA expression
CB NSCs
IVv NSCs
SVZ NSCs
CB
IVv
SVZ
NSCs
En1
En2
Pax3
Emx2
FoxG1
βactin
C
CB NSCs
IVv NSCs
SVZ NSCs
Pax3
D
CB
SVZ
En2
Emx2
ISH
E
CB
IV ventricle
SVZ
Pax3
FoxG1
IHC
F
CB NSC-derived tumor
GFP
GFP
G
CB/IVv NSCs
SVZ NSCs
Classic vs Desmoplastic
ES
MB classic
MB desmoplastic
Rank list (x1000)
Nominal p-value 0.018
FDR q-value 0.058
Nominal p-value 0.095
FDR q-value 0.109
C vs Shh
MB group C
MB Shh
Nominal p-value 0.035
FDR q-value 0.103
Nominal p-value 0.171
FDR q-value 0.162

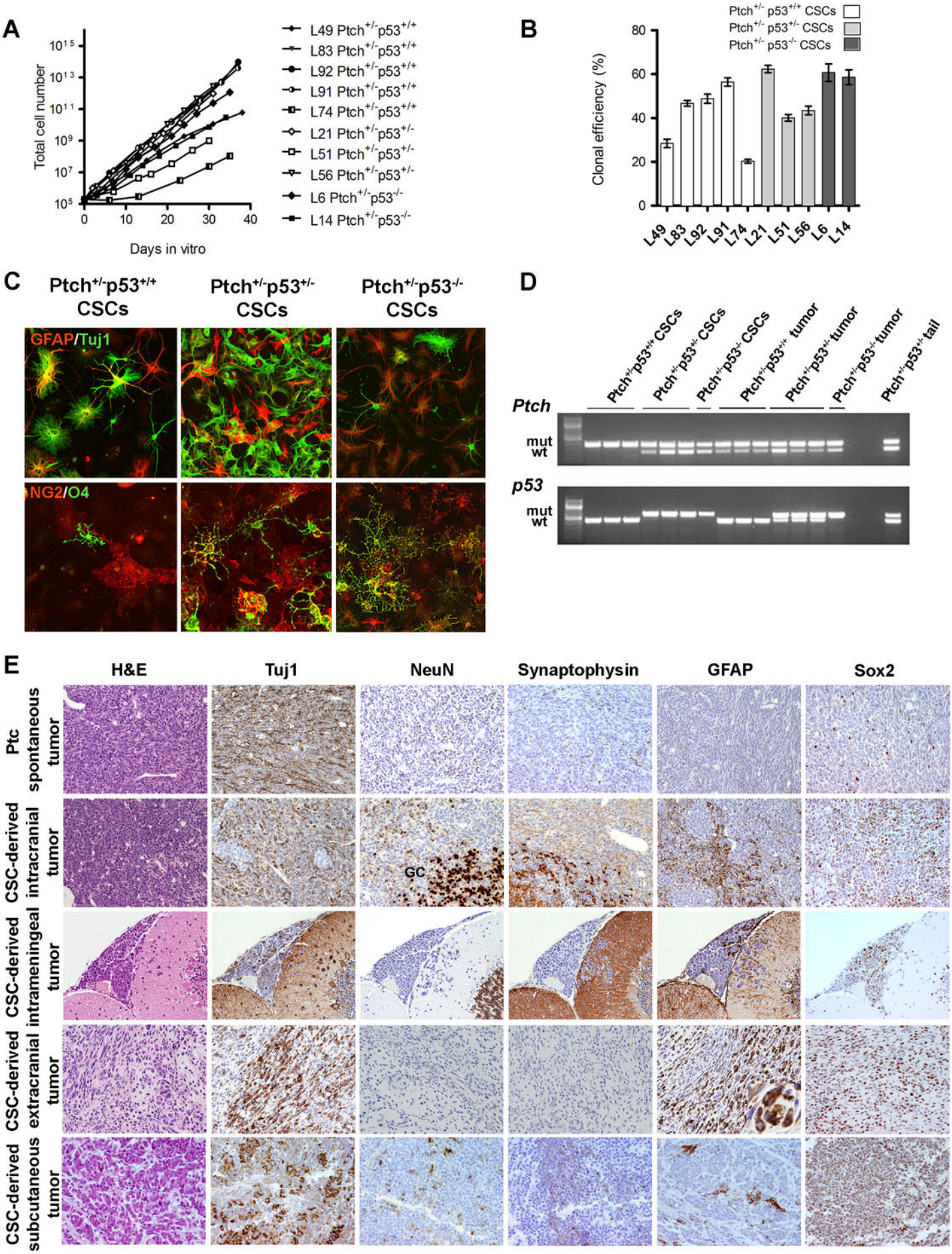
A
Total cell number
Days in vitro
L49 Ptch+/-p53+/+
L83 Ptch+/-p53+/+
L92 Ptch+/-p53+/+
L91 Ptch+/-p53+/+
L74 Ptch+/-p53+/+
L21 Ptch+/-p53+/-
L51 Ptch+/-p53+/-
L56 Ptch+/-p53+/-
L6 Ptch+/-p53-/-
L14 Ptch+/-p53-/-
B
Ptch+/- p53+/+ CSCs
Ptch+/- p53+/- CSCs
Ptch+/- p53-/- CSCs
Clonal efficiency (%)
L49 L83 L92 L91 L74 L21 L51 L56 L6 L14
C
Ptch+/-p53+/+ CSCs
Ptch+/-p53+/- CSCs
Ptch+/-p53-/- CSCs
GFAP/Tuj1
NG2/O4
D
Ptch+/-p53+/+ CSCs
Ptch+/-p53+/- CSCs
Ptch+/-p53-/- CSCs
Ptch+/-p53+/+ tumor
Ptch+/-p53+/- tumor
Ptch+/-p53-/- tumor
Ptch+/-p53+/- tail
Ptch
mut
wt
p53
mut
wt
E
H&E
Tuj1
NeuN
Synaptophysin
GFAP
Sox2
Ptc spontaneous tumor
CSC-derived intracranial tumor
GC
CSC-derived intrameningeal tumor
CSC-derived extracranial tumor
CSC-derived subcutaneous tumor

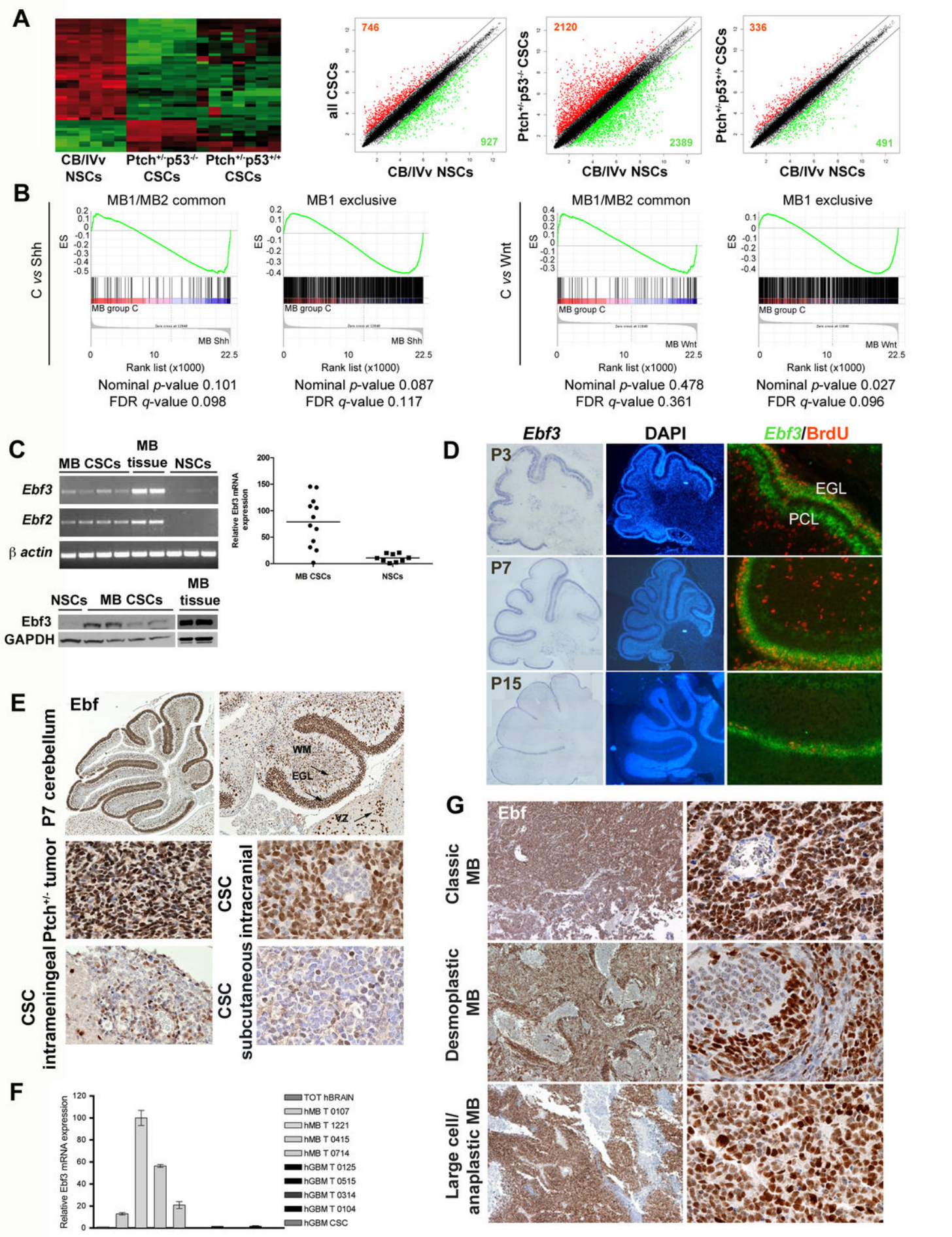
A
CB/IVv NSCs
Ptch+/-p53-/- CSCs
Ptch+/-p53+/+ CSCs
all CSCs
CB/IVv NSCs
746
927
Ptch+/-p53-/- CSCs
2120
2389
Ptch+/-p53+/+ CSCs
336
491
B
C vs Shh
MB1/MB2 common
MB1 exclusive
ES
MB group C
MB Shh
Rank list (x1000)
Nominal p-value 0.101
FDR q-value 0.098
Nominal p-value 0.087
FDR q-value 0.117
C vs Wnt
MB1/MB2 common
MB1 exclusive
MB Wnt
Nominal p-value 0.478
FDR q-value 0.361
Nominal p-value 0.027
FDR q-value 0.096
C
MB CSCs
MB tissue
NSCs
Ebf3
Ebf2
β actin
Relative Ebf3 mRNA expression
MB CSCs
NSCs
NSCs
MB CSCs
MB tissue
Ebf3
GAPDH
D
Ebf3
DAPI
Ebf3/BrdU
P3
P7
P15
EGL
PCL
E
Ebf
P7 cerebellum
WM
EGL
VZ
Ptch+/- tumor
CSC intracranial
CSC intrameningeal
CSC subcutaneous
F
Relative Ebf3 mRNA expression
TOT hBRAIN
hMB T 0107
hMB T 1221
hMB T 0415
hMB T 0714
hGBM T 0125
hGBM T 0515
hGBM T 0314
hGBM T 0104
hGBM CSC
G
Ebf
Classic MB
Desmoplastic MB
Large cell/ anaplastic MB

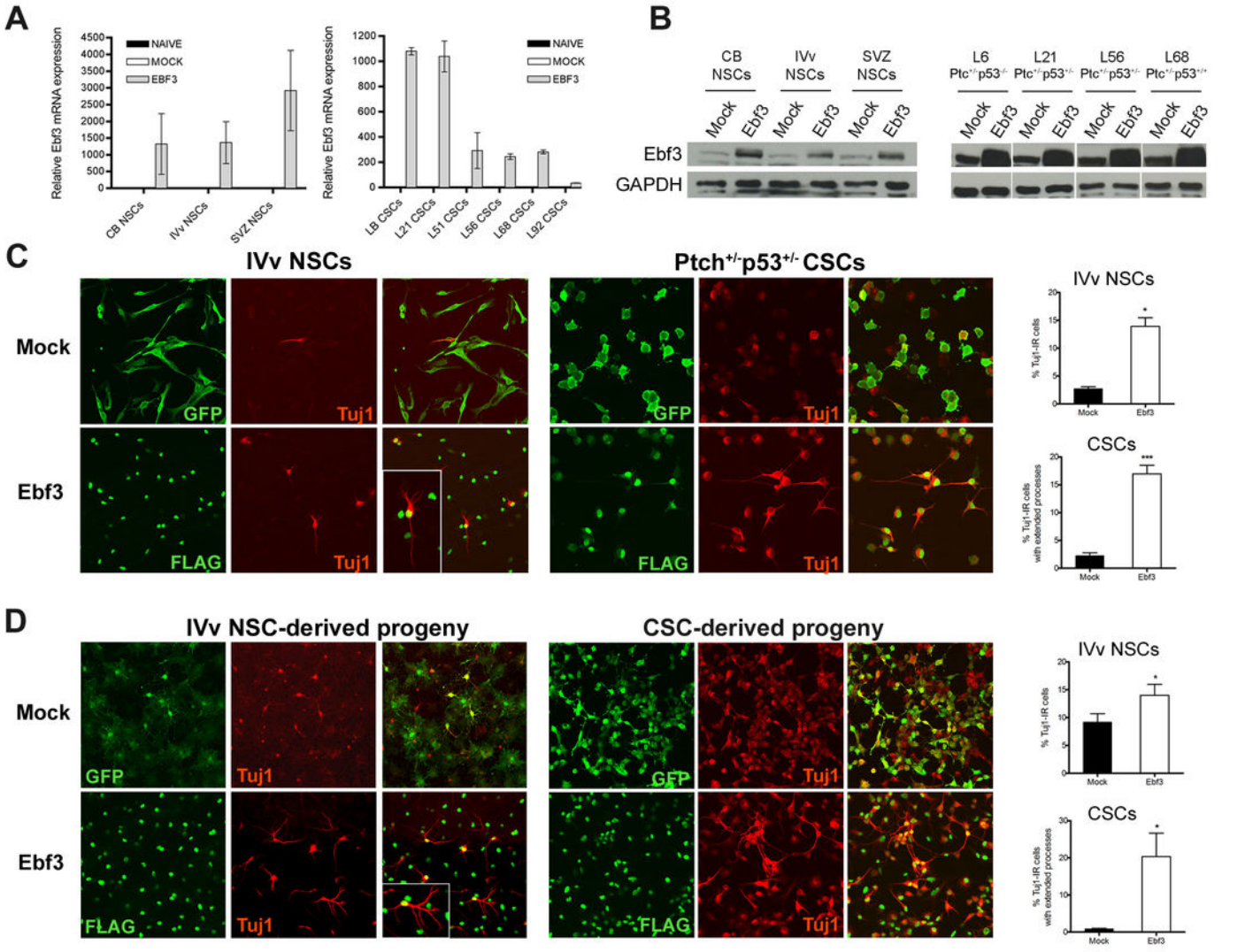
A
Relative Ebf3 mRNA expression
NAIVE
MOCK
EBF3
CB NSCs
IVv NSCs
SVZ NSCs
LB CSCs
L21 CSCs
L51 CSCs
L56 CSCs
L68 CSCs
L92 CSCs
B
CB NSCs
IVv NSCs
SVZ NSCs
L6 Ptch+/-p53-/-
L21 Ptch+/-p53+/-
L56 Ptch+/-p53+/-
L68 Ptch+/-p53+/+
Mock
Ebf3
GAPDH
C
IVv NSCs
Ptch+/-p53+/- CSCs
Mock
Ebf3
GFP
FLAG
Tuj1
% Tuj1-IR cells
% Tuj1-IR cells with extended processes
D
IVv NSC-derived progeny
CSC-derived progeny

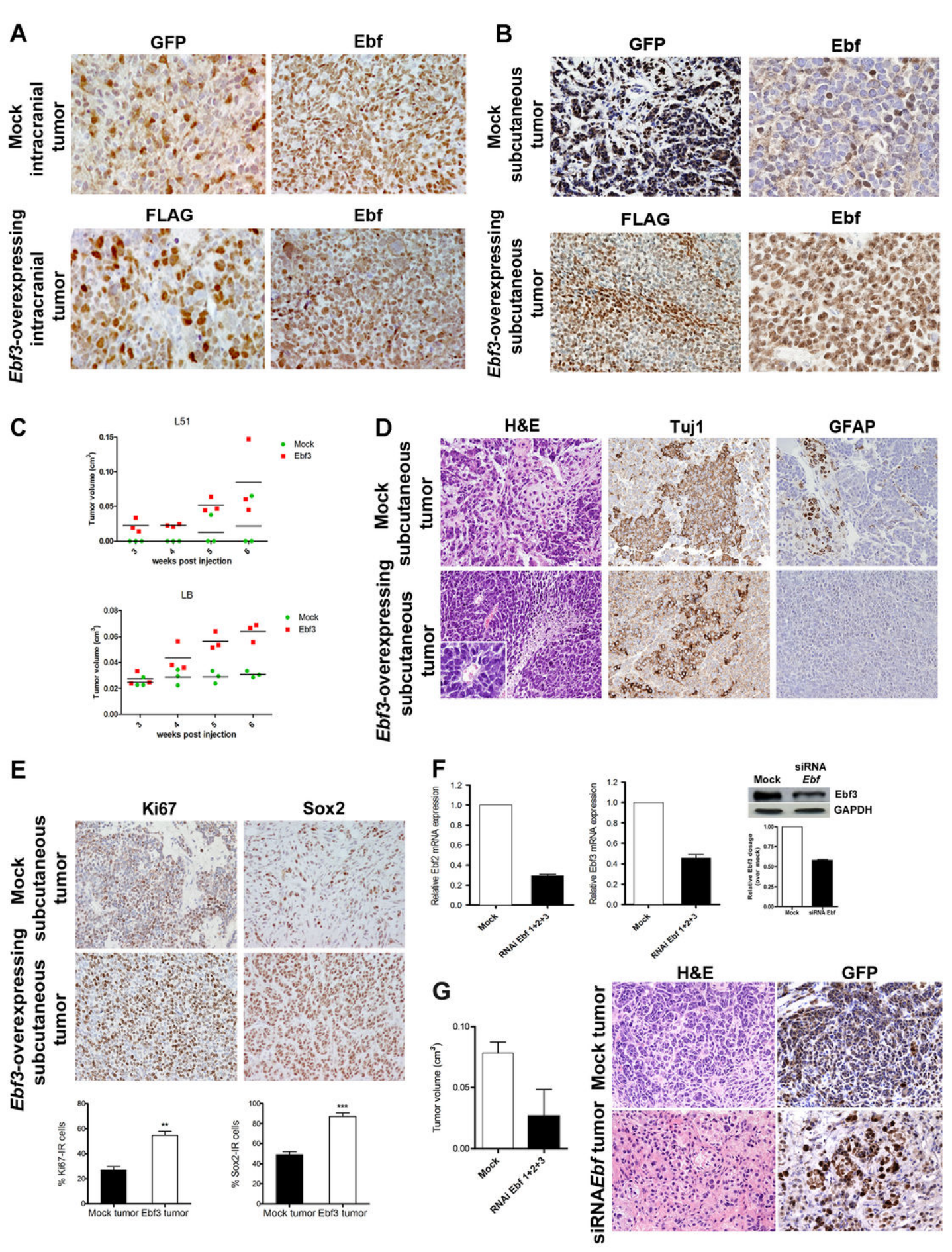
A
GFP
Ebf
Mock intracranial tumor
FLAG
Ebf
Ebf3-overexpressing intracranial tumor
B
GFP
Ebf
Mock subcutaneous tumor
FLAG
Ebf
Ebf3-overexpressing subcutaneous tumor
C
L51
Tumor volume (cm3)
0.15
0.10
0.05
0.00
3
4
5
6
weeks post injection
Mock
Ebf3
LB
Tumor volume (cm3)
0.08
0.06
0.04
0.02
0.00
3
4
5
6
weeks post injection
Mock
Ebf3
D
H&E
Tuj1
GFAP
Mock subcutaneous tumor
Ebf3-overexpressing subcutaneous tumor
E
Ki67
Sox2
Mock subcutaneous tumor
Ebf3-overexpressing subcutaneous tumor
% Ki67-IR cells
80
60
40
20
0
**
Mock tumor
Ebf3 tumor
% Sox2-IR cells
100
80
60
40
20
0
***
Mock tumor
Ebf3 tumor
F
Relative Ebf2 mRNA expression
1.2
1.0
0.8
0.6
0.4
0.2
0.0
Mock
RNAi Ebf 1+2+3
Relative Ebf3 mRNA expression
1.2
1.0
0.8
0.6
0.4
0.2
0.0
Mock
RNAi Ebf 1+2+3
siRNA
Mock
Ebf
Ebf3
GAPDH
Relative Ebf3 dosage (over mock)
1.00
0.75
0.50
0.25
0.00
Mock
siRNA Ebf
G
Tumor volume (cm3)
0.10
0.05
0.00
Mock
RNAi Ebf 1+2+3
H&E
GFP
Mock tumor
siRNAEbf tumor